An Adiabatic Linearized Path Integral Approach for Quantum Time-Correlation Functions II: A Cumulant Expansion Method for Improving Convergence

Maria Serena Causo and Giovanni Ciccotti

Dipartimento di Fisica, Università La Sapienza, Piazzale Aldo Moro 2, 00185 Roma, Italy

Sara Bonella*

NEST, Scuola Normale Superiore, Piazza dei Cavalieri 7, I-56126 Pisa, Italy

Rodolphe Vuilleumier

Dipartimento di Fisica, Università La Sapienza, Piazzale Aldo Moro 2, 00185 Roma, Italy, Université Pierre et Marie Curie, Laboratoire de Physique Théorique de la Matière Condensée, Case Courrier 121, 4 Place Jussieu, 75005 Paris, France

Received: March 20, 2006; In Final Form: May 10, 2006

Linearized mixed quantum-classical simulations are a promising approach for calculating time-correlation functions. At the moment, however, they suffer from some numerical problems that may compromise their efficiency and reliability in applications to realistic condensed-phase systems. In this paper, we present a method that improves upon the convergence properties of the standard algorithm for linearized calculations by implementing a cumulant expansion of the relevant averages. The effectiveness of the new approach is tested by applying it to the challenging computation of the diffusion of an excess electron in a metal−molten salt solution.

1. Introduction

Calculating quantum time-dependent quantities by computer simulation is a difficult task. The computational complexity of exact algorithms for integrating the appropriate evolution equations, in fact, grows exponentially with the number of degrees of freedom, thus limiting the usefulness of available methods to the study of relatively small systems. Consequently, many efforts are devoted to developing approaches that approximate the quantum evolution, reducing its computational cost as much as possible without compromising the accuracy of the simulation.

A popular avenue is to take some kind of classical limit for the dynamics of as many degrees of freedom as allowed by the characteristics of the system. Once that limit has been taken, standard techniques that have a polynomial scaling with the number of particles, e.g. molecular dynamics, can be applied to integrate the evolution equation of the classical subsystem. The evolution of the quantum degrees of freedom still requires the solution of a Schrödinger equation, but the dimensionality of the quantum problem is reduced to relatively few degrees of freedom whose description can be tackled numerically. Several such mixed quantum-classical methods exist: surface hopping, Ehrenfest dynamics, semiclassical initial value representation, and quantum-classical Wigner methods are just a few examples (for a review see, for example, ref 1). The main difference among these techniques lies in the way in which the classical limit for the bath is taken and, perhaps more importantly, in the coupling mechanism between the two subsystems.

Recently, a mixed quantum-classical scheme has been developed specifically to address the calculation of nonadiabatic quantum time-correlation functions in the condensed phase. The method, known as the linearized approach to nonadiabatic dynamics in the mapping formalism (LAND-Map),[2] builds on work by several groups,[3−9] and it has proved effective to capture the characteristics of the evolution of many nuclear degrees of freedom coupled to a two-level system in the presence of transitions among the electronic states.[10]

If the coupling between the classical and quantum subsystem is sufficiently small that the bath dynamics causes slow mixing of the quantum states on the time scales relevant to the measurement at hand, LAND-Map reduces naturally to an adiabatic propagation method.[11] In this limit, it has been applied to the study of the diffusion of an excess electron (the quantum subsystem) in a molten salt solution (the classical bath).[12] In the following, we shall refer to ref 12 as paper I. In paper I, it was shown that calculating correlation functions in the adiabatic linearized approximation requires propagating a set of interfering classical trajectories for the bath. The time-independent Schrödinger equation for the quantum particle depends parametrically on the position of the classical degrees of freedom and must also be solved at each time-step to determine the forces experienced by the bath. The correlation function is then obtained by averaging the contributions of appropriate quantities calculated along the trajectories.

The method outlined above is quite appealing from a conceptual viewpoint in that the approximations involved are well-defined and their validity can be tested in any application. Further, unlike other available algorithms, it preserves significant theoretical features of quantum statistical mechanics. For example, the Kubo relation among the position- and velocity-based estimators of the electron's diffusion is maintained within the limits imposed by the adiabatic approximation of the propagator.

* Corresponding author. s.bonella@sns.it.

10.1021/jp061725d CCC: $33.50
Published on Web 07/21/2006

Unfortunately, the numerical implementation of LAND-Map, both in its adiabatic and nonadiabatic versions, still suffers from numerical problems that may hinder its effectiveness in applications to systems with many degrees of freedom. The main difficulty arises from the nature of the quantities that must be averaged to obtain the correlation function. These depend on the electronic states and are, in general, complex functions of the nuclear variables. The presence of phase factors that can oscillate rapidly during the time evolution of the system is a serious complication in the evaluation of the average and it results in the fact that large error bars must be associated to the computation.

Attempts to remedy the situation by increasing the number of trajectories in the ensemble meet with another difficulty: the computational cost of quantum-classical trajectories. As mentioned before, although the evolution of the bath variables is classical, the forces along the trajectory are obtained by solving the time-independent Schrödinger equation for the quantum subsystem for both the ground and excited states. This implies the diagonalization of the quantum Hamiltonian at each time-step, an operation that increases the complexity of the evolution of the bath considerably with respect to the purely classical case in which the forces are derived from an empirical force field.

In this paper, we present a method that aims at taming the numerical difficulties described above by a different avenue. The idea is to use a cumulant expansion[13−15] of the relevant averages to abate the error associated with our estimate of the correlation function for any given ensemble size. Such an expansion has been used in the past to improve the convergence of averages of complex quantities, for example, in the calculation of the band profiles in Raman scattering from pure liquids.[16] Here, we explore its usefulness in the context of mixed quantum-classical calculations.

The paper is organized as follows: The form of the linearized adiabatic mixed quantum-classical time-correlation function is briefly reviewed in the first part of the Theory section and the cumulant method described in Section 2.2. Some arguments are then presented to justify the usefulness of the cumulant expansion for converging linearized calculations. In the Results section, we revisit the study of the diffusion of an excess electron in a metal−molten salt solution and apply the cumulant expansion to improve the convergence of the results previously obtained for this system. We show that, in this case, the error bars associated with the measurements are indeed reduced considerably compared to the "brute force" average procedure. Finally, a detailed description of some numerical aspects of the algorithm is presented in Appendix A.

2. Linearized Adiabatic Time-Dependent Quantum Correlation Function

2.1. Theory and Algorithm. In paper I, it was shown that, if the thermal wavelength of the classical bath is small, the linearized adiabatic approximation to the quantum time-correlation function of operators $\hat{A}$ and $\hat{B}$ is given by[12]

$$\langle \hat{A}\cdot \hat{B}(t)\rangle_{\mathrm{ad}}^{\mathrm{lin}} \sim \sum_i \sum_{i'} \int \mathrm{d}R_{ii'}(0) \int \mathrm{d}P_{ii'}(0)\, e^{-\beta\{P_{ii'}^2(0)/2M+E_i(R_{ii'}(0))\}} A_{ii'}^{\mathrm{w}}(R_{ii'}(0), P_{ii'}(0)) \times B_{i'i}^{\mathrm{w}}(R_{ii'}(t), P_{ii'}(t))\, e^{-i/\hbar\int_0^t \mathrm{d}t'\{E_i(R_{ii'}(t'))-E_{i'}(R_{ii'}(t'))\}} \quad (1)$$

In this expression, the sums on i and i' run over the quantum states, while $R_{ii'}(t)$ and $P_{ii'}(t)$ are the positions and momenta of the classical subsystem at time t as obtained by propagating a trajectory according to

$$M\frac{\mathrm{d}R_{ii'}}{\mathrm{d}t}(t) = P_{ii'}(t) \quad (2)$$

and

$$\frac{\mathrm{d}P_{ii'}}{\mathrm{d}t}(t) = F_{ii'}(R_{ii'}) \quad (3)$$

from a set of initial conditions $(R_{ii'}(0), P_{ii'}(0))$. In the above equation

$$F_{ii'}(R_{ii'}) = -\frac{1}{2}[\nabla_R E_i(R_{ii'}(t)) + \nabla_R E_{i'}(R_{ii'}(t))] \quad (4)$$

is the mean of the Helmann−Feynman force corresponding to surfaces i and i', and, for example, $E_i(R)$ is the ith eigenvalue of the electronic Hamiltonian at nuclear configuration R corresponding to the adiabatic basis set $|\Psi_i(R)\rangle$ that describes the quantum subsystem. The classical Boltzmann factor with "potential" $E_i(R)$ is the correct thermal weight for the correlation function if the temperature is high enough that the classical limit of the quantum thermal density can be taken. In the more general case, the Wigner transform (see below) of the product of the thermal density and operator $\hat{A}$ appears in the expression of the linearized correlation function. $A_{ii'}^{\mathrm{w}}(R_{ii'}(0), P_{ii'}(0))$ and $B_{i'i}^{\mathrm{w}}(R_{ii'}(t), P_{ii'}(t))$, defined as (for example)

$$A_{ii'}^{\mathrm{w}}(R_{ii'}(0), P_{ii'}(0)) = \int \mathrm{d}\xi\, e^{i/\hbar P_{ii'}(0)\xi} \left\langle R_{ii'}(0) + \frac{\xi}{2}, \Psi_{i'}(R_{ii'}(0))\right| \hat{A} \left|R_{ii'}(0) - \frac{\xi}{2}, \Psi_i(R_{ii'}(0))\right\rangle \quad (5)$$

are matrix elements in the electronic subspace of the partial Wigner transform with respect to nuclear variables of the operators $\hat{A}$ and $\hat{B}$.

Equation 1 is obtained from the standard expression of a time-correlation function for a system in thermal equilibrium

$$\langle \hat{A}\cdot \hat{B}(t)\rangle = \mathrm{Tr}\{\hat{\rho}\hat{A}\hat{U}^{\dagger}(t)\hat{B}\hat{U}(t)\} \quad (6)$$

if the Boltzmann density operator $\hat{\rho} = \exp[-\beta\hat{H}]/Z$ is dominated by diagonal elements in the bath coordinates representation. Such a limit is verified, for example, in the case of high temperatures. Under these circumstances, the path integral representation of the forward and backward propagators, $\hat{U}(t)$ and $\hat{U}^{\dagger}(t)$, can be conveniently expressed in terms of mean and difference paths. The phase of the time-correlation function is then expanded in the difference path and the expansion truncated to linear order. This allows performing the integrations over the difference path analytically, collapses the dynamics of the mean path to the classical-like evolution described by eqs 2 and 3, and introduces the Wigner transforms of the operators (see paper I for a detailed description of the procedure that leads to eq 1).

The algorithm for calculating the adiabatic linearized time-correlation function is in principle straightforward: (a) For every i, sample a set of initial conditions for the classical variables from the Boltzmann distribution corresponding to the Born−Oppenheimer surface E_i. (b) For every i', evaluate the partial Wigner transform of operator $\hat{A}$ at time zero, propagate the classical evolution equations on the average Born−Oppenheimer potential surface (i, i') as in eqs 2 and 3 using a standard integrator such as the Verlet algorithm, and accumulate the time integral of the energy gap along the trajectory. The evaluation

of the forces acting on the classical subsystem requires diagonalizing the electronic Hamiltonian. (c) Calculate the partial Wigner transform of operator $\hat{B}$ at the end point of the trajectory. (d) Repeat steps (a−c) for all trajectories and all pairs of electronic indexes and average until convergence.

Assuming that only the ground electronic state is thermally populated, the sum over i in eq 1 can be restricted to one term. This further approximation allows writing the correlation function as

$$\langle \hat{A}\cdot\hat{B}(t)\rangle_{\mathrm{ad}}^{\mathrm{lin}} \sim \sum_{i'} \frac{1}{Z_0}\int \mathrm{d}R_{0i'}(0)\int \mathrm{d}P_{0i'}(0)\; e^{-\beta\{P_{0i'}^2(0)/2M+E_0(R_{0i'}(0))\}}\, A_{0i'}^{\mathrm{w}}(R_{0i'}(0),P_{0i'}(0))\times B_{i'0}^{\mathrm{w}}(R_{0i'}(t),P_{0i'}(t))\, e^{-i/\hbar\int_0^t \mathrm{d}t'\{E_0(R_{0i'}(t'))-E_{i'}(R_{0i'}(t'))\}} \quad (7)$$

with $Z_0 = \int \mathrm{d}R_{0i'}(0) \int \mathrm{d}P_{0i'}(0)\; e^{-\beta\{P_{0i'}{}^2(0)/2M+E_0(R_{0i'}{}'(0))\}}$. The expression above is valid in a range of temperatures defined by two hypothesis. On one hand, the coordinate representation of the density matrix must be dominated by diagonal contributions for the linearization procedure to be accurate; on the other, the energy gap between the ground and excited electronic states must be large enough to make the thermal population of the excited states negligible. The first requirement sets a lower bound, related to the thermal wavelength of the classical subsystem, for the temperature, while the second establishes an upper limit based on the characteristics of the energy spectrum of the quantum subsystem. For every sampled initial condition on the ground-state Born−Oppenheimer surface, a large number of trajectories still need to be propagated to perform the sum on the index i' in the correlation function. In actual calculations, this sum is restricted to a set of electronic states chosen on the basis of appropriate convergence tests.

Notice that, even though we are considering an adiabatic limit for the dynamics (i.e., no electronic transitions are induced by the nuclear motion), the forces experienced by the classical bath in step (b) of the algorithm are determined by more than one quantum state: if $i \neq i'$ in eq 7, the classical evolution is governed by a potential given by the mean of the eigenvalues with indexes i and i'. This characteristic feature of a linearized time-correlation function results from the fact that the operators are still represented at the full quantum level. In particular, they can have nonzero off-diagonal matrix elements in the chosen electronic basis set. Contributions from such elements to the correlation function are weighted by a phase factor proportional to the time integral of the energy gap between the two states identified by the matrix elements of the operators. In general, as time goes by, the integral grows, inducing rapid oscillations of the phase of the off-diagonal terms of the correlation function. At long times, it becomes difficult to account properly for the interference effects determined by such oscillations in the average over trajectories. A typical consequence of these difficulties can be seen in Figure 5. The figure shows an estimate of the electron's diffusion in a metal−molten salt solution based on the velocity autocorrelation function of the quantum particle. Details of the calculation can be found in the Results section; here, we only point out the large error bars that must be associated with the measure (see inset) as a result of the oscillations of the phase factor.

When calculating a linearized correlation function, reducing the uncertainty on the average simply by increasing the number of trajectories in the ensemble is not a viable solution. The forces that govern the motion are determined by the gradients of the eigenvalues of the electronic Hamiltonian. These quantities must be obtained at each time-step by solving the appropriate time-independent Schrödinger equation. Even considering that, to get convergence, it is enough to include $i' < 10$ in eq 7, implementing the procedure described in the Appendix to obtain the forces and to accumulate the energy-gap-dependent phase factor along a trajectory makes the evolution of the bath variables in our correlation function considerably more expensive than a purely classical calculation. The results presented in Figure 5, for example, were obtained by propagating an ensemble of 2304 classical trajectories on a IBM p690 cluster. The total computer time needed, equivalent to that of the calculation on a single-processor PC, was 20 000 CPU hours. More than 90% of that time was devoted to obtaining the eigenstates of the system and to calculating the corresponding Hellmann−Feynman forces.

A better strategy to improve the convergence of a linearized calculation is to reduce the error associated with the average for a fixed ensemble size by summing the contributions to the observable in a more efficient way. In the next section, we present a possible avenue to pursue this goal based on the cumulant expansion of the linearized time-correlation function.

2.2. Cumulant Expansion. Let us consider a set of N random variables $\{X_1,..., X_N\}$. The moment-generating function for the probability distribution $P(X_1, ..., X_N)$ is defined as

$$M(\lambda_1, ..., \lambda_N) = \langle e^{\sum_{i=1}^N \lambda_i X_i}\rangle \quad (8)$$

Here, the bracket indicates an average over the distribution P. Given M, the moments of the distribution can be calculated by evaluating its derivatives for $\{\lambda\} = \{0\}$.

A useful characterization of the random variables and of the asymptotic properties of the distribution can also be obtained by introducing the cumulants.[13] These are defined in terms of a generating function, called the cumulant-generating function $R(\lambda_1, ..., \lambda_N)$, related to M by

$$R(\lambda_1, ..., \lambda_N) = \ln[M(\lambda_1, ..., \lambda_N)] \quad (9)$$

The cumulants are obtained as the partial derivatives of the generating function R calculated for $\{\lambda\} = \{0\}$, thus

$$\langle X_1{}^{\nu_1}, ..., X_N{}^{\nu_N}\rangle_{\mathrm{c}} = \left\{\frac{\partial^{\nu_1}}{\partial\lambda_1{}^{\nu_1}} \cdots \frac{\partial^{\nu_N}}{\partial\lambda_N{}^{\nu_N}} R(\lambda_1, ..., \lambda_N)\right\}_{\{\lambda\}=\{0\}} \quad (10)$$

By using the definitions above, the moment-generating function can be expressed in terms of the exponential of a series in the cumulants as

$$\langle e^{\sum_{i=1}^N \lambda_i X_i}\rangle = e^{\sum'_{\nu_1}\cdots\sum'_{\nu_2} \Pi_j(\lambda_j{}^{\nu_j}/\nu_j!)\langle X_1{}^{\nu_1}\cdots X_N{}^{\nu_N}\rangle_{\mathrm{c}}} \quad (11)$$

The prime indicates that term $\nu_1 = \nu_2 = ... = \nu_N = 0$ has been omitted from the sums.

Note that a cumulant of a given order is not a simple average, rather it can be expressed as a combination of moments of order lower or equal to its own. For example

$$\langle X_1X_2\rangle_{\mathrm{c}} = \frac{\partial}{\partial\lambda_1}\frac{\partial}{\partial\lambda_2}\ln[\langle e^{(\lambda_1X_1+\lambda_2X_2)}\rangle]|_{\lambda_1=\lambda_2=0} = \langle X_1X_2\rangle - \langle X_1\rangle\langle X_2\rangle \quad (12)$$

The effect of the combination is essentially to isolate the highest-order intrinsic correlation among the stochastic variables. Thus, if the variables are weakly correlated, the cumulant expansion in eq 11 can be expected to converge quite rapidly. In fact, it

can be proved[13] that a cumulant $\langle X_1 X_2 ... X_N \rangle_c$ is zero if the variables $\{X_1, X_2, ..., X_N\}$ can be divided in two or more statistically independent sets.

The properties of the cumulant expansion can be exploited to improve the convergence of the linearized calculation of a time-correlation function. Let us observe first that eq 7 can be written as

$$\langle \hat{A} \cdot \hat{B}(t) \rangle_{ad}^{lin} \sim \sum_{i'} \langle A_{0i'}^{w}(R_{0i'}(0), P_{0i'}(0)) B_{i'0}^{w}(R_{0i'}(t), P_{0i'}(t)) e^{-i/\hbar \int_0^t dt' \{E_0(R_{0i'}(t')) - E_{i'}(R_{0i'}(t'))\}} \rangle \quad (13)$$

where the average is taken with respect to the normalized probability density

$$P(R_{0i'}, P_{0i'}) = \frac{1}{Z_0} e^{-\beta \{P_{0i'}^2(0)/2M + E_0(R_{0i'}(0))\}} \quad (14)$$

Each term in the sum can then be cast in the form of the expectation value of an exponential thanks to the identity

$$\langle A_{0i'}^{w}(R_{0i'}(0), P_{0i'}(0)) B_{i'0}^{w}(R_{0i'}(t), P_{0i'}(t)) e^{-i/\hbar \int_0^t dt' \{E_0(R_{0i'}(t')) - E_i(R_{0i'}(t'))\}} \rangle = \frac{d}{d\epsilon} \langle e^{\epsilon A_{0i'}^{w}(R_{0i'}(0), P_{0i'}(0)) B_{i'0}^{w}(R_{0i'}(t), P_{0i'}(t)) - i/\hbar \int_0^t dt' \{E_0(R_{0i'}(t')) - E_{i'}(R_{0i'}(t'))\}} \rangle |_{\epsilon=0} \quad (15)$$

For each value of t, the exponent can be read as the sum of the stochastic variables

$$X_{1t} = A_{0i'}^{w}(R_{0i'}(0), P_{0i'}(0)) B_{i'0}^{w}(R_{0i'}(t), P_{0i'}(t))$$
$$X_{2t} = -\frac{i}{\hbar} \int_0^t dt' \{E_0(R_{0i'}(t')) - E_{i'}(R_{0i'}(t'))\} \quad (16)$$

(in the above expression, time plays the role of an external parameter and it does not indicate a time-dependent stochastic process). We can now use eq 11, with $\{\lambda_1, \lambda_2\} = \{\epsilon, 1\}$, to express the terms contributing to the linearized correlation function as a cumulant expansion

$$\frac{d}{d\epsilon} \langle e^{\epsilon X_{1t} + X_{2t}} \rangle |_{\epsilon=0} = \frac{d}{d\epsilon} \{ e^{\sum'_{\nu_1} \sum'_{\nu_2} (\epsilon^{\nu_1}/\nu_1! \nu_2!) \langle X_{1t}^{\nu_1} X_{2t}^{\nu_2} \rangle_c} \}_{\epsilon=0} \quad (17)$$

By evaluating the derivative with respect to ϵ and returning to the explicit form of the stochastic variables, we obtain

$$\langle A_{0i'}^{w}(R_{0i'}(0), P_{0i'}(0)) B_{i'0}^{w}(R_{0i'}(t), P_{0i'}(t)) e^{-i/\hbar \int_0^t dt' \{E_0(R_{0i'}(t')) - E_{i'}(R_{0i'}(t'))\}} \rangle = \left[\sum_{\nu_2} \frac{1}{\nu_2!} \langle A_{0i'}^{w}(R_{0i'}(0), P_{0i'}(0)) B_{i'0}^{w}(R_{0i'}(t), P_{0i'}(t)) (i \int_0^t dt' \Omega_{i'0}(t'))^{\nu_2} \rangle_c \right] \times e^{\sum'_{\nu} (1/\nu!) \langle (i \int_0^t dt' \Omega_{i'0}(t'))^{\nu} \rangle_c} \quad (18)$$

(see eqs 12 and 16 for the definitions of the cumulant average and of the stochastic variables X_1 and X_2 in the term in square brackets). In the expression above, we also introduced the positive definite quantity $\Omega_{i'0}(t') = \{E_{i'}(R_{0i'}(t')) - E_0(R_{0i'}(t'))\}/\hbar$.

The equation above is the main result of this paper: it provides us with an expression for the terms of the adiabatic linearized time correlation as a cumulant series. The convergence properties of the cumulant expansion cannot be assessed in general because they depend on the characteristics of the observables involved in the calculation, with particular reference to the statistical correlation of the partial Wigner transforms of the operators and the integral of the energy gap. All nondiagonal terms, however, are now multiplied by the exponential of the cumulant expansion of the energy gap integral rather than by the original phase factor on the right-hand side of eq 18. Some of the terms in the expansion produce damping factors that tend to zero quite rapidly exactly when the integral of the energy gap grows in time, creating the fast oscillations in the phase of the original expression of the linearized correlation function. As most time-correlation functions tend to zero at long times in condensed-phase systems, such factors may help in achieving convergence. In the next section, we present data for the calculation of the diffusion of an excess electron in a metal−molten salt solution that support this statement.

3. Model, Numerical Algorithms, and Results

The calculation of the diffusion properties of an excess electron in a metal−molten salt solution has known considerable theoretical and experimental[17,18] interest. In a series of papers,[19−23] a model for this problem, consisting of a system of 32 K^+ cations, 31 Cl^- anions, and 1 electron placed in a periodically repeated cubic box of length $L = 13.695$ Å, was defined. The interaction potential among the ions was chosen to be of the Born−Mayer[24] form

$$\Phi(\boldsymbol{R}) = \sum_{\vec{n}} \sum_{I \le J}' \left[A_{I,J} e^{-\alpha |R_I - R_J - \vec{n}L|} + \frac{Z_I Z_J e^2}{|R_I - R_J - \vec{n}L|} \right] \quad (19)$$

where e is the electron's charge, R_I is the position, and Z_I the valence of the Ith ion, $\vec{n} \in Z^3$, and $\sum'$ means that $I \neq J$ if $\vec{n} = \vec{0}$.

The parameters in the potential are those assigned by Sangster and Dixon[25]

$$\alpha = 2.967 \text{ Å}^{-1}$$

$$A_{I,J} = \begin{bmatrix} 248.9597 \times 10^{-18} \text{ J if } I \text{ and } J \text{ correspond to } K^+ \text{ ions} \\ 308.0966 \times 10^{-18} \text{ J if } I \text{ and } J \text{ correspond to } Cl^- \text{ ions} \\ 286.0371 \times 10^{-18} \text{ J if } I \text{ and } J \text{ correspond to different ion types} \end{bmatrix} \quad (20)$$

The sum over the periodically repeated cells was neglected for the exponentially decaying interaction terms of the potential in eq 19, while it was performed using the Ewald sum method for the Coulomb part.

In the model, the interaction among the ions and the electron was given by a smoothed Coulomb potential[20] with functional form

$$v(\boldsymbol{x}, \boldsymbol{R}) = \sum_{\vec{n}} \sum_{I} \frac{Z_I e^2}{|\boldsymbol{x} - \boldsymbol{R}_I + \vec{n}L|} \text{erf}\left(\frac{|\boldsymbol{x} - \boldsymbol{R}_I + \vec{n}L|}{\lambda_I} \right) \quad (21)$$

where erf(x) is the error function. The parameters are

$$Z_I = \begin{bmatrix} 1 \text{ if } I \text{ corresponds to } K^+ \text{ ions} \\ -1 \text{ if } I \text{ corresponds to } Cl^- \text{ ions} \end{bmatrix}$$
$$\lambda_I = \begin{bmatrix} 1.953 \text{ Å if } I \text{ corresponds to } K^+ \text{ ions} \\ 1.164 \text{ Å if } I \text{ corresponds to } Cl^- \text{ ions} \end{bmatrix} \quad (22)$$

The model described above was used by Selloni and coworkers,[26] in conjunction with an adiabatic propagation scheme different from the one discussed in this paper, to calculate the diffusion constant of the excess electron and the Franck−Condon approximation of the power spectrum of the electron's velocity autocorrelation function. In the calculation, the mass density was equal to $\rho = 1.52 \times 10^3$ kg/m^3, and the temperature was set to $T = 1300$ K. The results they obtained were in agreement with available experimental data.

In paper I, we used the same model to calculate the diffusion properties of the excess electron using the linearized adiabatic time-correlation function method discussed in the Theory section. In that calculation, we performed a brute force average of the correlation function, and although our results showed fair agreement with the available experimental and theoretical benchmarks, the quality of some of the data was not entirely satisfactory. In particular, large error bars were associated to the velocity-based estimator of the diffusion

$$D_v = \frac{1}{3}\,\mathrm{Re}\int_0^\infty C_{vv}(t)\,\mathrm{d}t \tag{23}$$

(as obtained by taking the $\omega \rightarrow 0$ limit of the Fourier transform of the Kubo transform of the velocity autocorrelation function[27]) due to the noise introduced at long times by the phase factors associated to the electron's velocity autocorrelation function

$$C_{vv}(t) = \langle \hat{v} \cdot \hat{v}(t)\rangle = \mathrm{Tr}\{\hat{\rho}\hat{v}\hat{v}(t)\} \tag{24}$$

in its linearized form. Because the power spectrum of the dipole autocorrelation is given by the Fourier transform of $C_{vv}(t)$

$$I(\omega) = \frac{1}{2\pi\omega^2}\int_{-\infty}^{\infty} C_{vv}(t)\, e^{-i\omega t}\,\mathrm{d}t \tag{25}$$

the rough quality of the data for the velocity autocorrelation function at long times was also reflected in large error bars associated with the power spectrum at small energies.

Here, we revisit the calculations performed in paper I with the intent to improve the statistical convergence of the results by processing the data used in that work with the cumulant expansion procedure. In this calculation, as in paper I, the electron is the quantum subsystem, while the ions represent the classical bath. To enforce the prescriptions of the algorithm described in the Theory section, we need to calculate the eigenvalues of the quantum subsystem, E_i, at each time-step along the classical trajectory of the ions. These quantities are necessary both to sample initial conditions for the ions (see point (a) in the algorithm) and to calculate the time integral of the energy gap along the trajectory. The eigenvalues and the eigenvectors are obtained by solving the time-independent Schrödinger equation

$$H_{el}(\boldsymbol{R}; x)\Psi_i(\boldsymbol{R}; x) = E_i(\boldsymbol{R})\Psi_i(\boldsymbol{R}; x) \tag{26}$$

for the electronic Hamiltonian obtained using the potentials in eqs 19 and 20. In the numerical implementation, the equation above is solved, after discretization on a real space grid, by using a block Lanczos diagonalization algorithm with restarting and selective reorthogonalization (see refs 28−32). The propagation of the evolution equations required by point (b) in the algorithm is performed with a velocity Verlet integrator. The coupled evolution of the classical bath and the quantum subsystem requires a small time-step, dt, to be captured accurately. In the calculations presented in the following we set $\mathrm{d}t = 5 \times 10^{-18}$ s. The Hellmann−Feynman forces in eq 3 are given by

$$F_{ii'}(\mathbf{R}) = -\nabla_{\mathbf{R}}\Phi(\mathbf{R}) - \frac{1}{2}\{\langle\Psi_i(\mathbf{R}; \mathbf{x})|\nabla_{\mathbf{R}}v(\mathbf{R}; \mathbf{x})|\Psi_i(\mathbf{R}; \mathbf{x})\rangle + \langle\Psi_{i'}(\mathbf{R}; \mathbf{x})|\nabla_{\mathbf{R}}v(\mathbf{R}; \mathbf{x})|\Psi_{i'}(\mathbf{R}; \mathbf{x})\rangle\} \tag{27}$$

The evaluation of the term in curly brackets is described in detail in the Appendix. Here, we mention that the term is obtained most efficiently by expanding the potential in eq 20 in a Fourier series, taking the gradient in the reciprocal space, performing the inverse Fourier transform, and calculating the integrals over the electronic positions on a grid. This procedure scales with the number of grid points, N, like N log N. In our case, $N = 32^3$. Consequently, the force calculation in our algorithm is more expensive than the one performed in a classical simulation that scales linearly with the number of propagated degrees of freedom. This fact, along with the diagonalization of the electronic Hamiltonian, increases the numerical cost of the evaluation of the linearized correlation function considerably with respect to the classical case.

The final ingredients required by the algorithm are the matrix elements in the quantum subspace of the partial Wigner transforms with respect to the bath coordinates of the operators at the initial and final times of the propagation, see points (a) and (c) in the Theory section. In the case of the electron's diffusion, these transforms are trivial. The relevant operator, the electron's velocity, is in fact independent of bath coordinates (or, equivalently, the operator is the tensor product of the quantum subsystem's velocity and the identity operator in the bath subspace), and the Wigner transforms coincide simply with the electron's velocity matrix elements in the chosen basis set.

Having illustrated the numerical procedure used to perform the steps described in the algorithm, let us now focus on the study of the properties of the cumulant expansion presented in the Theory section. We then specialize eq 18 to the case of the electron's velocity autocorrelation function and define

$$C^j_{vv}(t) \equiv \langle v_{0j}(0)v_{j0}(t)\, e^{i/\hbar\int_0^t \mathrm{d}t'\{E_j(R_{0j}(t'))-E_0(R_{0j}(t'))\}}\rangle = \left[\sum_{\nu_2}\frac{1}{\nu_2!}\langle v_{0j}(0)v_{j\,0}(t)\,(i\int_0^t \mathrm{d}t'\Omega_{j0}(t'))^{\nu_2}\rangle_c\right] e^{\sum'_\nu(1/\nu!)\langle(i/\int_0^t \mathrm{d}t'\Omega_{j0}(t'))^\nu\rangle_c} \tag{28}$$

The total correlation function can then be obtained simply as

$$C_{vv}(t) = \sum_{j=0}^{j\mathrm{max}} C^j_{vv}(t) \tag{29}$$

In the above expressions, j replaces the index i' used to indicate the second set of electronic states necessary to resolve the expression of the correlation function in the chosen basis set (see eq 1). The number of such states that must be included in the calculation depends on the nature of the observables being measured (see discussion of step (b) of the algorithm in the Theory section and the comments following eq 7) and on the nature of the energy spectrum that influences the sum through the phase factor containing the integral of the frequency Ω_{j0}. In the present calculation, we verified that convergence with respect to summation over the index j was obtained with $j$max $= 9$. Note also that, in line with the approximation introduced with eq 7, we have assumed that only the ground electronic state is thermally populated at the chosen temperature.

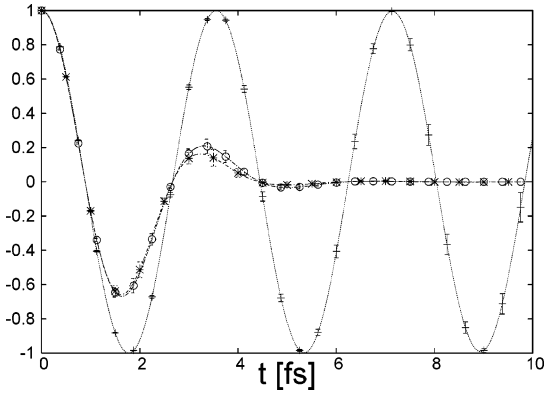

Figure 1. Real part of $g^1_{\nu^{max}}(t)$, see eq 29, for $\nu^{max} = 1$ (+), $\nu^{max} = 2$ (○) and $\nu^{max} = 6$ (∗). The estimates corresponding to $\nu^{max} = 2$ and $\nu^{max} = 6$ agree within error bars, but the statistical errors associated with g^1_6 are bigger than the ones associated with g^1_2. The differences in the error bars are more apparent around $t \approx 3.5$ fs, where the statistical errors associated with g^1_6 are 20% larger than those associated with g^1_2.

We now move to study the convergence of the cumulant expansion of the different j terms in the linearized time-correlation function. Let us begin by investigating the behavior of the series in ν in eq 27 because the exponential character of this factor should dominate the properties of the overall result. Let us then consider the quantity

$$g^j_{\nu^{max}}(t) = e^{\sum_{\nu=1}^{\nu^{max}} (1/\nu!)\langle (i\int_0^t d\tau \Omega_{0j}(\tau))^\nu\rangle_c} \qquad (30)$$

Figure 1 shows the real part of this function for $\nu^{max} = 1$, 2, and 6. In the figure, $j = 1$, but very similar behavior is observed for terms with a different electronic state index. As it can be seen from the figure, the convergence of $g^j_{\nu^{max}}(t)$ with respect to truncation in the sum is very rapid and an accurate value of the function is obtained already with $\nu^{max} = 2$, even at long times.

The situation is quite different if we consider the behavior of the other factor in eq 27. Let us define

$$I^j_{\nu_2^{max}} = \sum_{\nu_2=0}^{\nu_2^{max}} \frac{1}{\nu_2!} \langle v_{0j}(0) v_{j0}(t) \, (i \int_0^t d\tau \Omega_{j0}(\tau))^{\nu_2}\rangle_c \qquad (31)$$

Figure 2 presents the real part of the series above, for $\nu_2^{max} = 0$ (in which case, only the product of the electron's velocity at different times is averaged) and $\nu_2^{max} = 2$. Note that, because of the multiplicative imaginary unit appearing in it, the terms in the series are alternatively purely real or imaginary so that, to see a change in the real or imaginary parts of the series, it is necessary to increase the index ν_2 by two. As before, we set $j = 1$, but the results are qualitatively similar for other choices of this index. In this case, the successive terms do not appear to become small with increasing value of ν_2 and the convergence of the series is not apparent. In fact, successive terms can change the order of magnitude of the sum, as it can already be seen in the figure, where the amplitude of the result for $\nu_2^{max} = 0$ is dominated by that of the $\nu_2^{max} = 2$ to the point that it cannot be observed on the scale of the figure. However, Figure 3 shows that, when eqs 29 and 30 are multiplied, the exponential dominates and the result is stable for $\nu_2^{max} \geq 3$. In all calculations in the figure, we set $\nu = 2$; the different curves were obtained by varying the index ν_2^{max} from 0 to 4. The long time convergence of the results, controlled in all cases by the damping due to the exponential factor, is very rapid and the

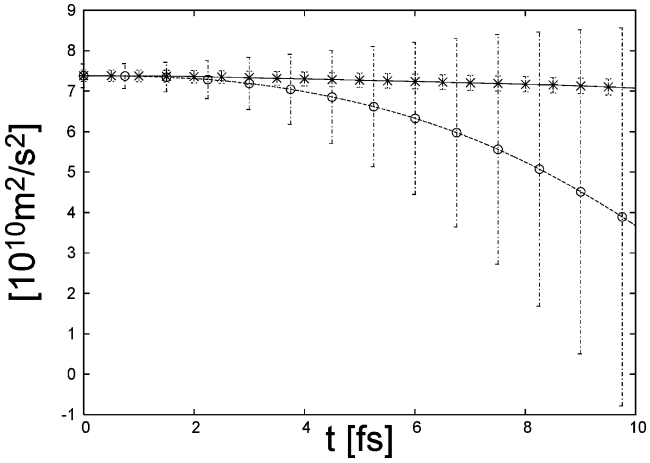

Figure 2. Real part of $I^1_{\nu_2^{max}}(t)$, see eq 30, for $\nu_2^{max} = 0$ (∗) and $\nu_2^{max} = 2$ (○). The amplitude of the two results differs by 1 order of magnitude. Note also the rapid increase of the error bars associated with the calculations. Terms with a larger value of ν_2^{max} show an even more rapid growth both in amplitude and in the error bars.

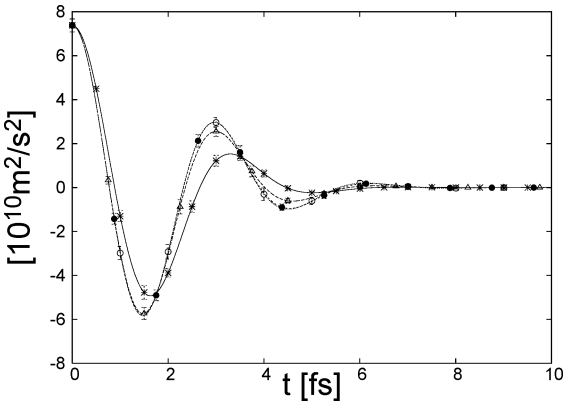

Figure 3. Real part of $C^1_{vv}(t)$ for $\nu_2^{max} = 0$ (∗), $\nu_2^{max} = 2$ (△), $\nu_2^{max} = 3$ (○), $\nu_2^{max} = 4$ (●), and $\nu^{max} = 2$. Convergence is much slower than it was for $g^1_{\nu^{max}}$. In the time region around $t = 4.5$ fs, the estimates corresponding to $\nu_2^{max} = 2$ still do not agree within error bars with the ones for $\nu_2^{max} = 3$, while the estimates corresponding to $\nu_2^{max} = 3$ and $\nu_2^{max} = 4$ are in agreement in the full time range. The error bars associated with $\nu_2^{max} = 3$ and $\nu_2^{max} = 4$ are comparable.

curves coincide for all values of the index ν_2^{max}. At shorter times, on the other hand, the competition between the two factors in the product is visible in the slight shift to the left of the minimum after $t = 4.5 \times 10^{-15}$ s and in the increase in the depth of the corresponding peak. The maximum around $t = 3 \times 10^{-15}$ s is also shifted to the left, and the height of the peak increases slightly. Similarly, the minimum at about $t = 1.5 \times 10^{-15}$ s becomes deeper as we include more terms in the sum.

Nevertheless, these effects do not change the overall behavior of the cumulant expansion, and the results for $\nu_2^{max} = 3$ and $\nu_2^{max} = 4$ are equal within error bars. It is interesting to notice that the terms $\nu^{max} = 2$ and $\nu_2{}^{max} = 0$ correspond to an expansion of the terms in the correlation function of the following form

$$C^j_{vv;2}(t) = \langle v_{0j}(0) v_{j0}(t)\rangle_c \, e^{\sum_{\nu=1}^{2} (1/\nu!)\langle (i\int_0^t d\tau \Omega_{j0}(\tau))^\nu\rangle_c} \qquad (32)$$

This expression is akin to the second-order cumulant expansions that have appeared in the literature, for example, in calculations of time-correlation function within the formalism of centroid path integrals proposed by Voth and co-workers[33,34] or in the

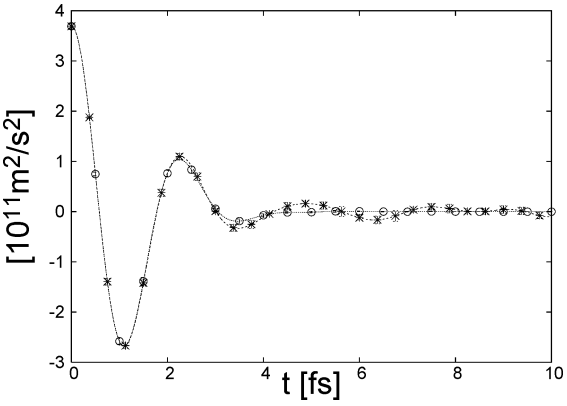

Figure 4. Real part of the electron's velocity adiabatic linearized autocorrelation function. Just a few points with error bars are plotted for the estimates coming from the method presented in this paper (○) and from the brute force average (∗) of the correlation function presented in paper I.

simulation of the dynamics of a solvated electron in water by Staib and Borgis.[35] In these applications, the cumulant expansion is truncated at second order based on two hypothesis. The first one is that the complex exponential and the product of operators (a feature common to the approximations just mentioned and our method despite the relevant differences in the prescriptions for the time evolution in the distinct approaches) can be treated as essentially independent statistical variables so that the cumulant average can be factorized as the product of two terms. In the simulation of the solvated electron, for instance, this amounts to the so-called vibration−rotation hypothesis. In that case, the operators are transition moments, which are assumed to depend mainly on orientation, while Ω depends on vibrations, and the two show little reciprocal dependence. The second hypothesis is that the distribution of the random variable Ω can be effectively approximated by a Gaussian probability, so that the expansion in the exponential can be truncated at second order without loss of accuracy (a second-order cumulant expansion is exact for Gaussian processes). Figure 1 shows that, for the present calculation, truncating the exponential sum at second order is indeed a good approximation. However, the hypothesis of de-correlation at this low order in the overall cumulant expansion does not seem to be verified, at least at short time, for the velocity autocorrelation function. The curve marked with the asterisks in Figure 3, which corresponds to the second-order term, shows clear deviations from the converged results both in the position and in the height of the peaks for $t \leq 5 \times 10^{-15}$ s. As the nature of these peaks is crucial for the numerical value of the integral of the velocity autocorrelation function, and thus for the value of the electron's diffusion constant, we must conclude that the usual second-order cumulant expansion is not adequate in this case.

Terms with $j \neq 1$ in the expression for the time-dependent correlation function $C_{vv}(t)$ behave similarly with respect to convergence with the index ν_2^{max}.

Having verified the convergence of the cumulant expansion, we now compare the linearized velocity autocorrelation function obtained with the procedure described in this paper to the one resulting from the "brute force" averaging of eq 7. Figure 4 shows the behavior of the real part of $C_{vv}(t)$ in the two cases. The initial features of the two curves coincide within error bars because the oscillations induced by the integral of the energy gap in the brute force average are not particularly severe at short times. The long-time behavior of the two estimators, however, differs considerably. While the result of the cumulant average converges to zero at $t = 4 \times 10^{-15}$ s, the standard average continues to oscillate, overemphasizing correlations in the system. The characteristics of the imaginary part of the correlation functions (not shown) are similar.

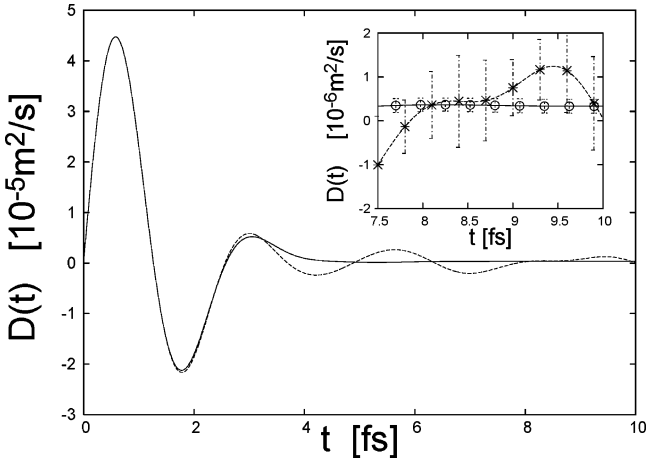

Figure 5. Electron's diffusion coefficient as a function of the upper limit of the time integration used in the simulation. The full line identifies the curve obtained with the cumulant expansion method, while the dashed one corresponds to the standard approach. The inset magnifies the long time behavior of the two estimators. Just a few points and the associated error bars are shown for the estimates with (○) and without (∗) cumulant espansion.

The improvement produced by the cumulant averaging procedure becomes manifest when we calculate the electron's diffusion coefficient and the power spectrum. Figure 5 displays the diffusion coefficient obtained via eq 22 as a function of the upper limit of the time integration used in the simulation. Reflecting the properties of the correlation function, the two curves agree at short times. For $t \geq 3 \times 10^{-15}$ s, however, the pathologies of the standard treatment become more difficult to control and the estimator used in paper I shows persistent oscillations that make it difficult to obtain a reliable measure of the diffusion. The data processed with the cumulant expansion method, on the other hand, converge very rapidly to a stable plateau value of $D = (3.0 \pm 1.5) \times 10^{-7}$ m^2 s^{-1}, in excellent agreement with the experimental value[17] $D_e = 3 \times 10^{-7}$ m^2 s^{-1}. For completeness, we also report the value $D_s = 2 \times 10^{-7}$ m^2 s^{-1}, obtained for the same model employed here but via a different estimator, by Selloni and co-workers.[26] The uncertainty in our measure is still quite large due to the relatively small size of the ensemble used in the simulation. The enhancement of the quality of the result is, however, apparent if one looks at the inset in the figure, which magnifies the behavior of the two estimators at the longer times. It should also be pointed out that the cumulant expansion allows reaching of the plateau value for the diffusion integral at shorter times so that the costly diagonalization procedure necessary for the calculation of the forces and described in the Appendix needs to be performed for a smaller number of time-steps. Thus, it becomes possible to improve the result further by increasing the number of trajectories in the ensemble. Finally, notice that the results presented here were obtained by processing the *same* set of data either with the method described in this paper or with the standard average procedure of paper I. The focus of the present work is on exploring the effect of the cumulant expansion on averages obtained for fixed ensemble size. The convergence of a given linearized calculation with ensemble size depends, of course, on the nature of system and of the observables that appear in the correlation function. For a fixed number of electronic states (index j in eq 28), the statistical errors decrease

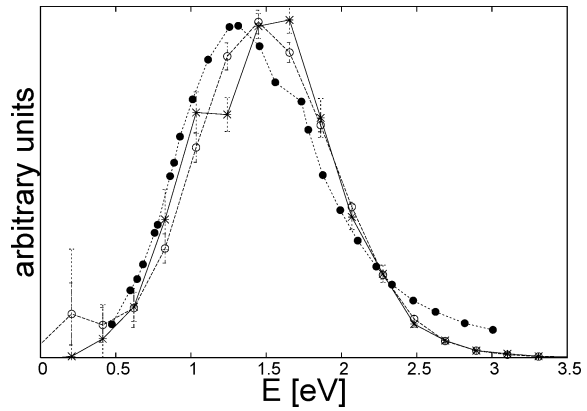

Figure 6. Comparison of power spectra. Results from the present calculation (○) are connected by the dashed line, while the calculations performed in paper I (∗) are connected by a full line. In both calculations, the temperature is $T = 1300$ K. Experimental results (● connected by the dotted curve) at $T = 1133$ K[18] are also displayed.

with the number of trajectories, N, as $1/\sqrt{N}$. In the case of the present calculation, we did not repeat the study of the convergence with respect to the number of trajectories that was performed to obtain the results presented in paper I. Rather, we used a set of fixed size (2304 trajectories) that had given reasonably well-converged results for the brute force average procedure and tested the improvement achieved through the cumulant expansion.

To conclude, in Figure 6, we present a comparison of the power spectrum calculated with and without the cumulant expansion. We also compare our calculations to the experimental power spectrum obtained by Freyland and co-workers[18] at the slightly lower temperature $T = 1133$ K. The calculated line widths agree well with the experiment, while the peaks obtained by simulation are slightly shifted toward higher energy. The numerical data treated with the cumulant expansion produces a smoother band than the one resulting from a standard average. In particular, the spurious shoulder appearing between 0.9 and 1.25 eV in the "standard" band is completely removed by the new averaging procedure.

4. Conclusions

A new method for improving convergence of adiabatic linearized time-correlation functions, based on an exact rewriting of the linearized correlation function in terms of a cumulant expansion, has been presented in this paper. The method's efficacy in controlling the phase oscillations associated to the standard expression of the correlation function has been tested by using it to reduce substantially the error associated with the estimate of the diffusion coefficient of an excess electron in a metal−molten salt solution. General statements on the convergence properties of the cumulant expansion for arbitrary observables and systems are difficult to make and the effectiveness of the procedure must be analyzed on a case by case basis. However, some features of the method are encouraging in view of further applications. In particular, the cumulant expansion transforms the purely oscillatory factor related to the time integral of the electronic's states energy gap in the original expression for the linearized correlation function in a complex exponential whose real part provides some helpful damping terms. The oscillatory factor is the main source of difficulties in achieving convergence in the standard calculation, and it is a ubiquitous characteristic of the adiabatic linearized correlation functions, independent of the specific operators involved in the calculation. An analogous phase factor is also present in nonadiabatic generalizations of the theory. The fact that the exponential damping that helps in achieving fast convergence in the cumulant average originates precisely from this omnipresent foe suggests that the improvement observed in the calculations presented in this work may be preserved in other applications.

Acknowledgment. We wish to acknowledge many useful discussions with David Coker on linearized correlation functions. We would also like to thank Daniel Borgis, who was the first to suggest that a cumulant expansion might prove useful in these calculations. R.V.'s visit in Rome was partly supported by CASPUR. The use of computer time on the machines in CINECA and at the Forschungszentrum Jülich is also gratefully acknowledged.

A. Detailed Description of Some Aspects of the Numerical Procedure

A.1. Discretization of the Time-Independent Schrödinger Equation. To solve numerically the differential equations eq 26, we need to choose a discretization method and write H_{el} as a finite matrix. Let us then superimpose a cubic lattice with spacing $a = L/M$ on the simulation box. In our calculation, $M = 32$. The possible values of the variable $\mathbf{x}$ are then restricted to the $N = M^3$ lattice grid points. The eigenvalue problem (eq 26) takes the form

$$\sum_{\vec{m}} H^{d}_{\vec{n},\vec{m}}(\mathbf{R})\, \psi^{d}_{i\vec{m}}(\mathbf{R}) = E^{d}_{i}(\mathbf{R})\, \psi^{d}_{i\vec{n}}(\mathbf{R}) \tag{33}$$

where H^d, the discrete version of H_{el}, is a $N \times N$ real matrix, $E^d_i(\mathbf{R})$ is the ith eigenvalue associated with the N-dimensional real eigenvector $\psi^d_i(\mathbf{R})$ of components $\vec{n} = (n_1, n_2, n_3)$, $n_i = -M/2, \cdots, M/2 - 1$, The matrix H^d is the sum of two terms, the discrete representation of the potential operator, V^d, which is a diagonal real matrix, and the lattice representation of the kinetic operator K^d

$$H^{d}_{\vec{n},\vec{m}}(\mathbf{R}) = V^{d}_{\vec{n},\vec{n}}(\mathbf{R})\, \delta_{\vec{n},\vec{m}} + K^{d}_{\vec{n},\vec{m}} \tag{34}$$

where

$$K^{d}_{\vec{n},\vec{m}} = -\frac{\hbar^2}{2m_e a^2}[(\delta_{\vec{n},\vec{m}+\vec{e}_1} + \delta_{\vec{n},\vec{m}-\vec{e}_1} - 2\delta_{\vec{m},\vec{n}}) + (\delta_{\vec{m},\vec{n}+\vec{e}_2} + \delta_{\vec{m},\vec{n}-\vec{e}_2} - 2\delta_{\vec{m},\vec{n}}) + (\delta_{\vec{m},\vec{n}+\vec{e}_e} + \delta_{\vec{m},\vec{n}-\vec{e}_3} - 2\delta_{\vec{m},\vec{n}})] \tag{35}$$

and $\vec{e}_1 = (1, 0, 0)$, $\vec{e}_2 = (0, 1, 0)$, $\vec{e}_3 = (0, 0, 1)$. Periodic boundary conditions impose $\psi^d_{i\vec{m}+\vec{l}M} = \psi^d_{i\vec{m}}$ for any $\vec{l} \in Z^3$. Thus, in eq 35, we set $m_i + 1 = -M/2$, if $m_i = M/2-1$, and $m_i - 1 = M/2-1$, if $m_i = -M/2$.

The diagonal matrix V^d is the sum of the discrete representation of the Fumi−Tosi and ions−electron interaction operators. The discretization of the Fumi−Tosi potential (eq 21) is trivial and is given by $\Phi^d(\mathbf{R}) = \Phi(\mathbf{R})\, I_N$, where I_N is the $N \times N$ identity. The discretization of the smoothed Coulomb potential (eq 21), on the other hand, is more delicate. Because the potential in eq 21 is long-range, we need a prescription to carry out the infinite sum over periodically repeated cells. $v(\mathbf{x},\mathbf{R})$ has exactly the same form of the interaction potential of an electron with a periodically repeated ionic charge distribution

$$\rho(\mathbf{x}) = e \sum_{\vec{n}} \sum_{I} Z_I \left(\frac{1}{\lambda_I^2 \pi}\right)^{3/2} e^{-(\mathbf{x}-\mathbf{R_I}+\vec{n}L)^2/\lambda_I^2} \tag{36}$$

As such, it coincides with the long-range part of the Coulomb potential coming out from the Ewald sum method associated with Gaussian charge distributions of widths λ_I. Thus, it can be written in terms of a fast-converging Fourier series as

$$v(\mathbf{x}, \mathbf{R}) = -\frac{e^2}{L^3}\sum_{\vec{k}_{\vec{n}}\neq\vec{0}}\left[\frac{4\pi}{k_{\vec{n}}^2}\sum_I Z_I\, e^{i\vec{k}_{\vec{n}}\cdot\mathbf{R_I}} e^{-k_{\vec{n}}\lambda_I^2/4}\right] e^{-i\vec{k}_{\vec{n}}\cdot\mathbf{x}} = \sum_{\vec{k}_{\vec{n}}\neq\vec{0}}\sum_I f(\vec{k}_{\vec{n}}; \mathbf{R_I})\, e^{-i\vec{k}_{\vec{n}}\cdot\mathbf{x}} \quad (37)$$

where $\vec{k}_{\vec{n}} = 2\pi\vec{n}/L$, with $\vec{n} \in Z^3$. Thus, we can calculate the values assumed by the function v on the N points of the real space discretization lattice by performing a discrete Fourier antitransform, i.e., we consider only the N terms of the above Fourier series corresponding to those $\vec{k}_{\vec{l}}$ with $l_i = -M/2, \cdots, M/2 - 1$ and compute

$$v_{\vec{n}}^{\,d}(\mathbf{R}) = \sum_{\vec{k}_{\vec{l}}\neq\vec{0}}\sum_I f(\vec{k}_{\vec{l}}; \mathbf{R_I})\, e^{-i\vec{k}_{\vec{l}}\cdot\mathbf{x}_{\vec{n}}} \quad (38)$$

where $\mathbf{x}_{\vec{n}} = (an_1, an_2, an_3)$, with $n_i = -M/2, \cdots, M/2 - 1$ and a lattice spacing. This is done by using a fast Fourier transform routine, requiring a CPU time of order $N \log N$. Thus, the matrix V^d has the form $V^d = \Phi^d(\mathbf{R}) + v^d(\mathbf{R})$, where $\Phi^d_{\vec{n},\vec{m}}(\mathbf{R}) = \Phi(\mathbf{R})\delta_{\vec{n},\vec{m}}$ and $v^d(\mathbf{R}) = v_{\vec{n}}^{\,d}(\mathbf{R})\delta_{\vec{n},\vec{m}}$

A.2. Evaluation of the Hellmann−Feynman Forces. Finally, we describe how we computed the Hellmann−Feynman forces in eq 27. The contribution of the gradient of the Fumi−Tosi potential to the force can be calculated trivially. The forces associated to the smoothed Coulomb ions−electron interaction, on the other hand, require the knowledge of the quantum electronic eigenstates on a grid (see eq 27 and the discussion that follows). The discretized eigenvectors are available to us after implementing the Lanczos procedure. The operator $\nabla_{\mathbf{R_I}} v(\mathbf{x}, \mathbf{R})$, which also appears in eq 27, can be easily put in a discretized form following the same procedure used in order to discretize $v(\mathbf{x}, \mathbf{R})$. Because, from eq 37, it follows that $\nabla_{\mathbf{R_I}} v(\mathbf{x}, \mathbf{R}) = \sum_{\vec{k}\neq\vec{0}} i\vec{k}_{\vec{n}}\, f(k_{\vec{n}}; \mathbf{R_I})\, e^{-i\vec{k}_{\vec{n}}\cdot\mathbf{x}}$, the discretized version of the operator can be simply computed as

$$(\nabla_{\mathbf{R}_I} v(\mathbf{R}))^d_{\vec{n},\vec{m}} = \sum_{\vec{k}_{\vec{l}}\neq\vec{0}} i\vec{k}_{\vec{l}}\, f(\vec{k}_{\vec{l}}, \mathbf{R_I})\, e^{-i\vec{k}_{\vec{l}}\cdot\mathbf{x}_{\vec{n}}}\delta_{\vec{n},\vec{m}} \quad (39)$$

using a Fast Fourier antitransform on the reciprocal lattice associated with the discretization grid, as it was done for $v(\mathbf{x}, \mathbf{R})$. The contribution of state i to the Hellmann−Feynman force can then be computed as

$$\langle\Psi_i(\mathbf{R}; \mathbf{x})|\nabla_{\mathbf{R_I}} v(\mathbf{R}; \mathbf{x})|\, \Psi_i(\mathbf{R}; \mathbf{x}) \approx a^3 \sum_{\vec{n}} |\psi^d_{i\vec{n}}|^2\, (\nabla_{\mathbf{R_I}} v(\mathbf{R}))^d_{\vec{n},\vec{n}} \quad (40)$$

References and Notes

(1) Stock, G.; Thoss, M. *Adv. Chem. Phys.* **2005**, *131*, 243.
(2) Bonella, S.; Montemayor, D.; Coker, D. *Proc. Natl. Acad. Sci. U.S.A.* **2005**, *102*, 6715−6719.
(3) Hernandez, R.; Voth, G. *Chem. Phys. Lett.* **1998**, *223*, 243.
(4) Poulsen, J.; Nyman, G.; Rossky, P. *J. Chem. Phys.* **2003**, *119*, 12179.
(5) Shi, Q.; Geva, E. *J. Chem. Phys.* **2003**, *118*, 8173.
(6) Zhang, S.; Pollak, E. *J. Chem. Phys.* **2003**, *118*, 4357.
(7) Thoss, M.; Wang, H.; Miller, W. *J. Chem. Phys.* **2001**, *114*, 47.
(8) Sun, X.; Wang, H.; Miller, W. *J. Chem. Phys.* **1998**, *109*, 7064.
(9) Stock, G.; Thoss, M. *Phys. Rev. Lett.* **1997**, *78*, 578.
(10) Bonella, S.; Coker, D. F. *J. Chem. Phys.* **2005**, *122*, 194102.
(11) Coker, D.; Bonella, S. In *Computer Simulations in Condensed Matter: from Materials to Chemical Biology*; M. Ferrario, K. B., Ciccotti, G., Eds.; Springer: New York, 2006.
(12) Causo, M. S.; Ciccotti, G.; Montemayor, D.; Bonella, S.; Coker, D. *J. Phys. Chem. B* **2005**, *109*, 6855.
(13) Kubo, R. *J. Phys. Soc. Jpn.* **1962**, *17*, 1100.
(14) Kubo, R. *J. Math. Phys.* **1963**, *4*, 174.
(15) Mukamel, S. *Principles of Nonlinear Optical Spectroscopy;* Oxford University Press: Oxford, 1999.
(16) Bratos, S.; Tarjus, G. *Phys. Rev. A* **1981**, *24*, 1591.
(17) Bredig, M. *Molten Salt Chemistry;* Interscience: New York, 1964.
(18) Freyland, W.; Garbade, K.; Pfeiffer, E. *Phys. Rev. Lett.* **1983**, *51*, 1304.
(19) Parrinello, M.; Raman, A. *J. Phys. Chem.* **1984**, *80*, 860.
(20) Selloni, A.; Car, R.; Parrinello, M.; Carnevali, P. *J. Phys. Chem.* **1987**, *91*, 4947.
(21) Xu, L.; Selloni, A.; Parrinello, M. *Chem. Phys. Lett.* **1989**, *162*, 27.
(22) Fois, E.; Selloni, A.; Parrinello, M.; Car, R. *J. Phys. Chem.* **1988**, *92*, 3268.
(23) Fois, E.; Selloni, A.; Parrinello, M. *Phys. Rev.* **1989**, *39*, 4819.
(24) Fumi, F.; Tosi, M. *J. Phys. Chem. Solids* **1964**, *25*, 31.
(25) Sangster, M.; Dixon, M. *Adv. Phys.* **1976**, *25*, 247.
(26) Selloni, A.; Carnevali, P.; Car, R.; Parrinello, M. *Phys. Rev. Lett.* **1987**, *59*, 823.
(27) Kubo, R. *Rep. Prog. Phys.* **1966**, *29*, 255.
(28) Golub, G. H.; vanLoan, C. F. *Matrix Computations;* Johns Hopkins University Press: Baltimore, MD, 1996.
(29) Cullum, J.; Donath, W. E. In *Proceedings of the 1974 IEEE Conference on Decision and Control*; IEEE Press: New York, 1974.
(30) Pollard, W.; Friesner, R. *J. Chem. Phys.* **1993**, *99*, 6742.
(31) Wilkinson, J. *The Algebraic Eigenvalue Problem;* Clarendon Press: Oxford, 1965.
(32) Frenkel, D.; Smit, B. *Understanding Molecular Simulation*; Academic Press: New York, 1996.
(33) Cao, J.; Voth, G. *J. Chem. Phys.* **1994**, *100*, 5106.
(34) Hernandez, R..; Cao, J.; Voth, G. *J. Chem. Phys.* **1995**, *103*, 5018.
(35) Staib, A.; Borgis, D. *J. Chem. Phys.* **1995**, *103*, 2642.